Electronic Supplementary Material (ESI) for Physical Chemistry Chemical Physics.

Supporting information

Energy scales and dynamics of electronic excitations in functionalized gold nanoparticles measured at the single particle level

Tuhin Shuvra Basu,[1] Simon Diesch,[1] Manuel Obergfell,[2] Jure Demsar,[2] Elke Scheer[1]

[1]Department of Physics, University of Konstanz, 78457 Konstanz, Germany

[2]Institute of Physics, Johannes Gutenberg-University Mainz, 55128 Mainz, Germany

A. HR-TEM of Au NPs before functionalization

We have collected the aliquot of Au NPs (in water) prior to the final functionalization step to see the difference. The HR-TEM micrographs of Au NPs dissolved in water (without DT functionalization) are shown in Figure S1(a)-(d). We observe an uncontrolled growth of the Au NPs if they are not functionalized before the final cooling of the solvent. Correspondingly, they show a slightly higher size dispersion. We also observe that the stability of the non-functionalized Au NPs is much lower. They start to agglomerate, as seen in Fig. S1(b) and (d). Therefore, functionalization is beneficial to form a stable DBTJ for further studies using STM.

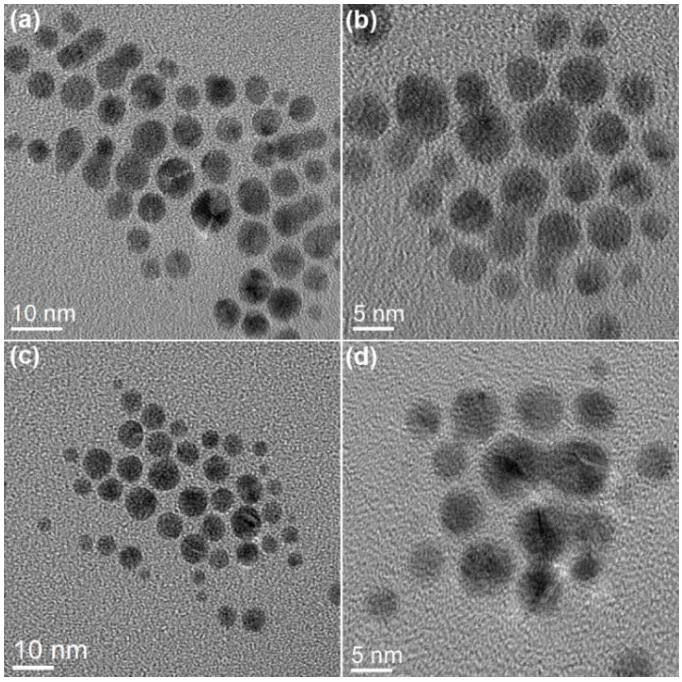

Fig. S1. (a)-(d) The HR-TEM images present the distribution of Au NPs in water before DT functionalization. (a) and (c) represent two different portions of the TEM grid with same batch whereas (b) and (d) exhibit the agglomeration with time.

B. Steady state absorption before and after functionalization

Fig. S2 presents background solvent corrected steady-state absorption spectra of Au NPs before and after DT attachment, dissolved in water and hexane, respectively. For bare Au NP, we observe the absorption peak centred at 528 nm, which is a

characteristic of LSPR. NPs with DT capped exhibits a LSPR peak blue shifted by 8 nm. Shift in the SPR peak position in the absorption characteristics of the metallic NPs can occur for many reasons e.g. size of the NPs, dielectric mismatch between the NPs and the surroundings, types of the inorganic or organic capping layer, thermal and electrical conductivity of the outer layer etc.[1-4]

Despite the fact of having slightly higher dielectric constant of the surroundings we observe a nominal blue shift in the LSPR peak position of capped Au NPs (refractive index of DT and hexane are 1.459 and 1.375, respectively and that of DI water is 1.333).[2, 4] This unusual phenomenon is rare but not impossible. For both bare and capped Au NPs, the size dispersion of Au NPs appears to be slightly on the higher size regime (see HR-TEM in the main text - Fig. 1a). The presence of higher sized Au NPs creates a red-shift in the SPR peak of bare Au NPs. The red-shift in the bare Au NPs occurs due to classical size effect as SPR peak position red shifts with increasing size. Whereas the observed blue shift, anomaly to the size effect, in the capped Au NPs takes place due to reduction of the electrical conductivity in the outermost capping layer.[4] Therefore, an overall 8 nm blue-shift can be foreseen in capped Au NPs ensemble compared to their bare counterpart. The slight broadening of the LSPR of the bare Au NPs can be attributed to both the enhanced LSPR dephasing rate and to the difference in the dielectric constants of the solvents in the two cases.[2, 3] The ligand, 1-dodecanethiol, does not affect the absorbance of the NPs in this spectral range as it has no pronounced absorption features.[5] We observe about 25% difference in the maximum absorption at 400 nm for the two solutions with identical molar concentrations of NPs. Since the concentrations of NPs are the same for both bare and capped NPs, the excitation densities should be comparable, unless the capping would have an influence on the excitation cross section. Thus, we attribute the higher absorption of the capped NPs (in hexane) to the stronger absorption of hexane. The second possible reason for the increased absorption can be the difference in dielectric constants and their mismatch with the electronic properties of the NPs. To summarize, the difference in absorption cannot account for the observed dramatic change of the electron dynamics discussed in the main text.

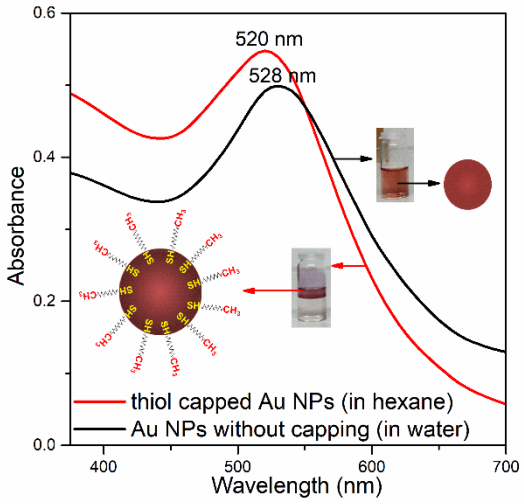

Fig. S2. The steady state absorption of the Au NP before and after thiol attachment in water and hexane, respectively. The blue shift in LSPR peak is consistent with thiol capping of the Au NPs.

C. Capacitance calculation of the DBTJ arrangement

We calculate the tunnelling capacitances by approximating the tip apex by a sphere and the surface by a plane. The capacitance beween tip and NP is approximated by a sphere-sphere geometry and the capacitance between NP and substrate by a sphere-plane geometry.[6]

$C_2 = 4\pi\varepsilon_0 r_{\mathrm{NP}} \sinh\alpha \sum_{n=1}^{\infty} \frac{1}{\sinh(n\alpha)}$ 1

Here $\alpha = \ln\left(\frac{l}{r_{\mathrm{NP}}} + \sqrt{\frac{l^2}{r_{\mathrm{NP}}^2} + \frac{2l}{r_{\mathrm{NP}}}} + 1\right)$ and *l* is the distance between the Au NP and substrate. r_{NP} is the radius of the Au NP. Eq. 1 is an infinite series, but summing up to 10 < *n* < 20 is sufficient for the present conditions. For $l < r_{NP}$, the equation simplifies to:

$C_2 \sim 2\pi\varepsilon_0 r_{\mathrm{NP}} \left[\ln\left(\frac{l}{r_{\mathrm{NP}}}\right) + \ln 2 + \frac{23}{20}\right]$ 2

The approximate solution of sphere-sphere capacitance, C_1, can be written in terms of C_2 with a correction factor *ß*:

$C_1\,(r_{\mathrm{tip}}, r_{\mathrm{NP}},\ l) = \gamma C_2\ (r_{\mathrm{NP}}, \beta l)$ 3

where r_{tip} is the apex radius of the tip and $\gamma = 1/\left\{1 + \left(\frac{r_{\mathrm{NP}}}{r_{\mathrm{tip}}}\right)\right\}$.

The calculated capacitances for our case are 0.15 aF (C_1) and 0.18 aF (C_2).

D. Level spacing of individual Au NP

The level spacing of spin-degenerate energy levels can be estimated by, $E_d \approx (2\pi^2\hbar^2/m_e k_F V)$, where ħ is the reduced Planck constant, m_e is the electron mass and k_F is the Fermi vector (for Au it turns out to be 1.21 × 10^{-10} m^{-1}).[7, 8] For a spherical Au NP, we have the volume $V = (4/3)\pi r_{\mathrm{NP}}^3$. E_d should be 1.9 meV for an average 6.0 nm Au NP. We cannot resolve these small energy spacings in the STS.

E. Featureless STS of DT functionalized Au NPs for large distances between the tip and the NP

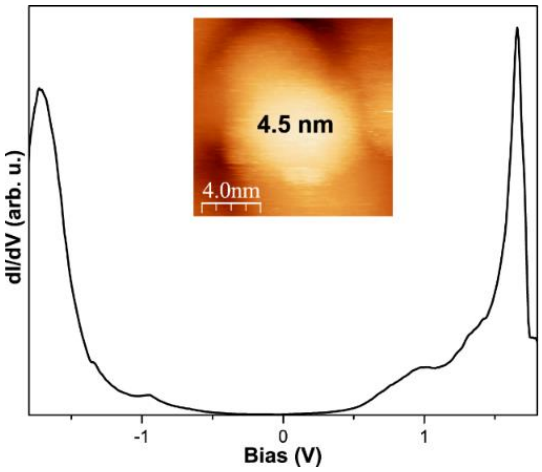

Fig. S3. STS of single Au NP (diameter 4.5 nm) with comparatively large tip-to-sample distance. STS has no features except for the reduced conductance at low bias typical for tunnelling transport.

An important factor to get a proper STS reflecting the electronic structure of the Au NPs is the choice of the tunnelling parameters, especially the resistance that is given by the tip and the sample distance. We observe that, when the distance between the tip and the sample becomes larger, the characteristic spectral features of the Au NP are lost. Fig. S3 presents the STS characteristics of such a junction. The tunnelling resistance is intentionally kept at 5.8 GΩ. Here, we observe a similar gap of around 0.7 V corresponding to the DT-functionalized Au NP, though we cannot calculate the gap precisely due to the strong exponential increase of the conductance.

F. Modification in the STS of DT functionalized Au NPs due to networking

As we discussed in the main text, Au NPs often build networks via self-assembly. The observed STS in such cases do not reflect the characteristics of individual Au NP; rather they show a modification of the STS due to the vicinity of other NPs. One of the representative images is shown in the Fig. S4.

In case of networks we observe pronounced differences between the conductance curves. E.g. NP 1 does not exhibit any blockade whereas NP 2 and 3 show zero conductance gaps around zero bias. The values do not mimic the blockade of the individual NP. The changes in the ZCG and other characteristics compared to isolated NPs may occur for several reasons. Most likely, the STS of the individual NP are modified due to changes of the tunnelling capacitances that arise from interactions between the neighbouring NPs surrounding the NP under study. These competing processes are, however, difficult to disentangle.

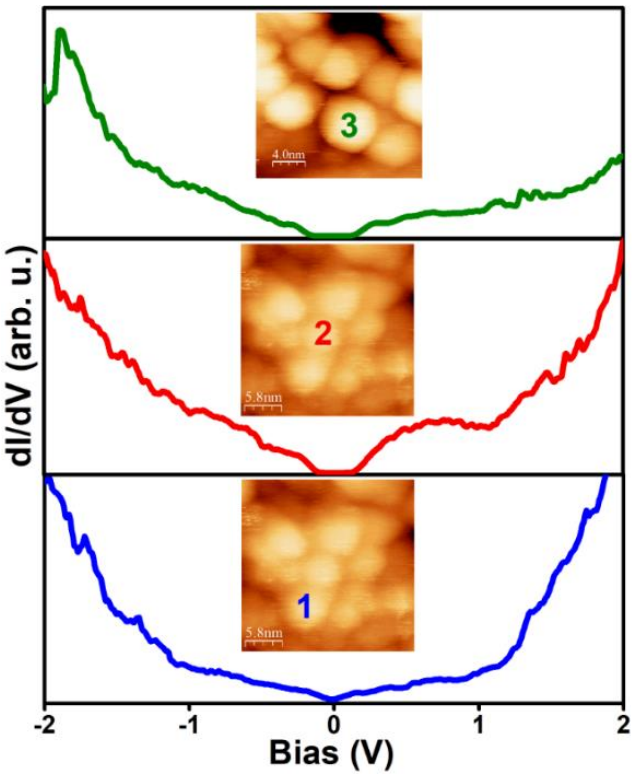

Fig. S4. STS of Au NPs that form a network. Au NP 1 and 2 (marked in the figure) are two different NPs in same network, whereas Au NP 3 is from a different network. The particle and the corresponding conductance curves are marked by different colours and the numbers.

G. Detection method of probing the STS of individual Au NP

Due to lower contrast between the Au NP and the substrate shown in the main text (Fig. 4c and 4d) we take tunnel spectra at several locations around the NP to gain the knowledge of the STS of the substrate. Therefore, we first scan a small area to locate the NP. Then we measure the size of the NP from the height profile analysis. Further, to make sure that the STS features originate from the NP we perform the STS surrounding the NP. Fig. S5a represents the conductance data of the Au (111) substrate and Fig. S5b is the conductance data of the HOPG substrate. Differential conductance of both substrates exhibits the characteristics of Au (111) and of HOPG. We did not see any special features related to the Au NP. The numbers in the figures indicate the positions where the STS has been performed. In conclusion, the findings indicate that the features in the STS shown in the main text are solely originating from the individual functionalized Au NP.

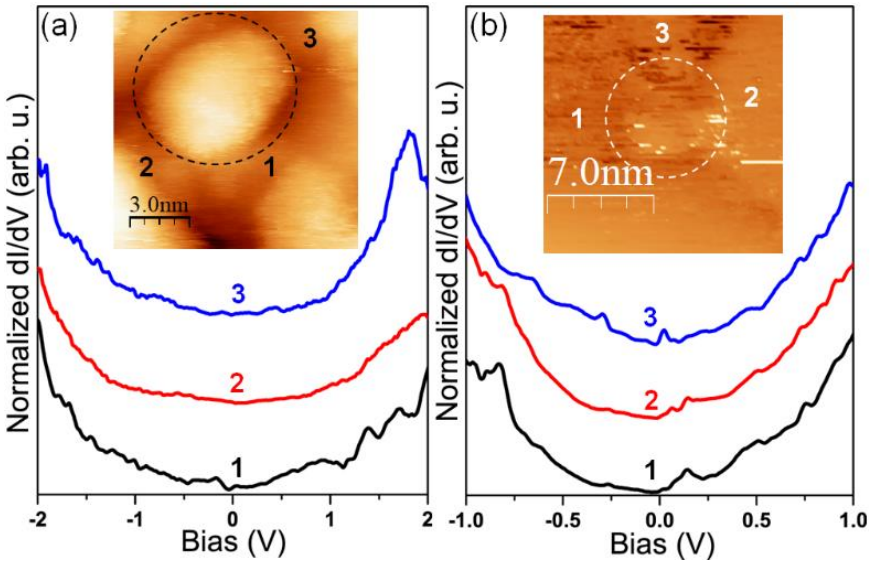

Fig. S5. Differential conductance of the nearby points surrounding the Au NP. The points of the conductance curves of (a) Au (111) and (b) HOPG substrate have been highlighted by the consecutive numbers.

H. Reproducibility of the STS of functionalized Au NP

To check the reproducibility of the Coulomb blockade and the subsequent staircases we perform differential conductance of other Au NPs.

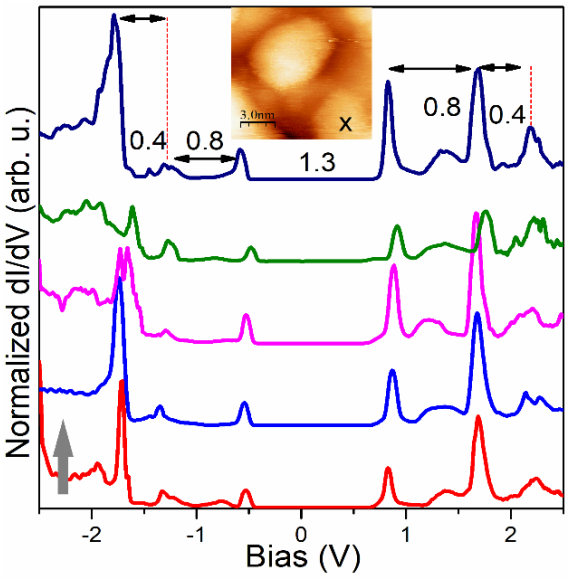

Fig. S6. Differential conductance of another functionalized Au NP marked by x. The different traces have been taken subsequently with the same tunnelling parameters at the same spot and show the stability and reproducibility of the measurement. Traces have been vertically offset for clarity.

The reproducibility of the STS is of good quality. The stable acquisition depends on many factors, like good tip condition, good choice of the tunnel resistance, a stable NP and on the substrate smoothness. The repetitive observation of the staircases as shown in the manuscript is more sensitive to the above factors compared to the simple Coulomb blockade region that we get regularly. Despite the sensitivity, we manage to acquire stable spectra shown in Fig. S6. The functionalized Au NP has been marked by 'x'. To demonstrate the reproducibility of the features, we show several successively recorded

conductance spectra (the arrows indicate the time direction; the experimental conditions were kept constant). The process has already been stated in the main text. The Coulomb blockade and the subsequent values of the staircases are in accordance to the physical phenomena discussed in the main text. The differences in the blockade and staircases values are due to the smaller size of the Au NPs.

I. Calculation of the residual charge

Q_0 is the fractional residual charge inside the NP and $Q_0(mod\ e)$ can be determined by the following equation:[9, 10]

$$Q_0 = \frac{1}{e}[C_2(\Delta\Phi_2) - C_1(\Delta\Phi_1)] \quad (4)$$

Here $\Delta\Phi_1$ and $\Delta\Phi_2$ are the contact potentials across the tunnel junctions 1 and 2.

J. Effect of residual charge on the Coulomb blockade due to the substrate alteration

As we discussed in the main text, when we replace the substrate by HOPG, the size of the Coulomb blockade gap has been reduced. We attribute this reduction to the effective residual charge inside the Au NP. The presence of the induced charge in the system becomes prominent when the potential of the NPs departs from zero when applying a bias. For unequal coupling strength between substrate and NP, and NP and tip, the effective potential of the NP varies, such that one probes the so-called Coulomb diamond under an angle (when change substrate to HOPG), as depicted in Fig. S7 by the dashed red line. The term Coulomb diamond denotes the shape of areas with constant ground state charge in a diagram of current vs source-drain (bias) voltage and a hypothetical gate voltage (determining the effective induced charge on the NP). Due to the asymmetric tunnelling conditions, i.e. $C_1 \neq C_2$, the effective charge varies when changing the bias voltage.

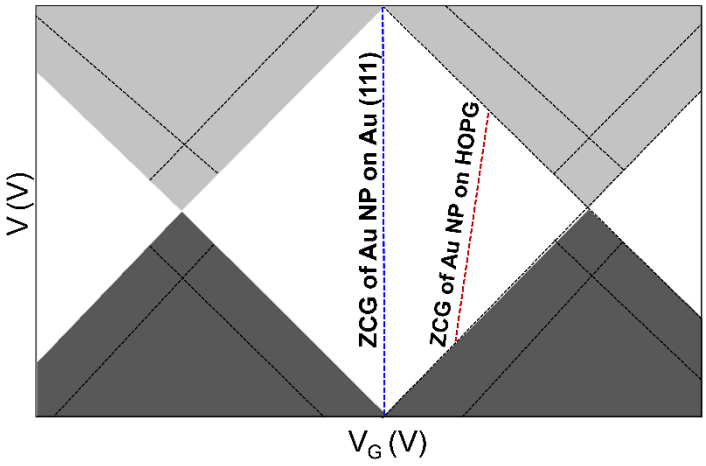

Fig. S7. Scheme of a Coulomb diamond, e.g. a current (grey areas with opposite sign in positive and negative polarity of bias voltage) vs. the source drain voltage V_{SD} and the gate voltage V_G. In the present experiment there is no V_G applied explicitly, but the effective gate voltage is determined by capacitively induced charges. The blue dotted line indicates the probing of Au NP on Au and the red symbolizes the probing of Au NP on HOPG substrate. For details see text. The thin black lines indicate inelastic excitations.

K. DT functionalized Au NP fabrication

DT functionalized Au NPs are fabricated following methods described elsewhere[11, 12] but are adapted to our experimental prerequisites. The fabrication involves several steps. We initially fabricate Au NPs (dispersed in water) from the reduction of

gold salt ($AuCl_3$) by sodium borohydride ($NaBH_4$). In a typical batch, first, a stock solution of 20 mM chloroauric acid ($HAuCl_4$) is prepared by mixing equimolar $AuCl_3$ and HCl. A stock solution of 20 mM reducing solvent is achieved by mixing $NaBH_4$ granules with the same molar NaOH solution. An aliquot of 100 µL of $HAuCl_4$ is taken in a pre-cleaned glass vial. The deionized water is added to have 10 g of solution. The whole mixture is stirred, and 700 µL of reducing solvent is dropwise added. The entire solution is heated to 100^{o}C and kept at this temperature for 5 min. The colour changes from pale yellowish to ruby red, confirming the presence of Au NPs in water. The volumetric ratio of $HAuCl_4$ and $NaBH_4$/NaOH is significant to control the size of the Au NPs. In our case, the ratio is kept at 7:1. During the synthesis, the pH of the solution is maintained at 7, and the entire reaction is performed under N_2 using a Schlenk line. We obtain an ensemble of bare Au NPs in water without any attached organic functional groups. Surface functionalization is necessary to have stable, monodisperse and well-separated Au NPs for STS measurements. To this end, 5 g acetone is added to bare Au NP solution while stirring for 2 min. We add 5 g of hexane with 1 µM of 1-DT while stirring for 1 min. Thereby the Au NPs are functionalized and are rapidly attached with the sulphur (S) of thiol moieties by a strong chemisorption mechanism. The processes yield two layers in the vial. The top layer consists of ruby red DT functionalized Au NP and the bottom is a colourless acetone-water mixture (see inset of Fig. S2). The upper layer is extracted using a micro-syringe and finally is collected after passing through a 0.22 µm pore sized polyvinylidene fluoride (PVDF) membrane to remove agglomerated unreacted organic portions.

L. Substrate preparation for STM

The scanning region for tunnelling measurements is limited to an area of about (1 µm x 1 µm) by the lateral scan range of our STM.[13] In the present study, we scan individual areas as small as (50 nm x 50 nm) because of the limited scan speed and the small sizes of NPs. For this reason, NPs on the substrate must be well distributed and well attached to the substrate to find them within the smallest scan area. The substrate is an atomically flat Au (111) thin film deposited on mica from Phasis Sàrl, Switzerland. To make a thin monolayer, we put a toluene droplet on Au (111) substrate and put a droplet of Au NP (in hexane) on top.[11] The hexane evaporates faster than toluene; thus, Au NPs freely move at the toluene-air interface. A thin monolayer of Au NPs is obtained after drying in the oven at 60°C. The prepared films have been transferred to the STM chamber which is brought to cryogenic vacuum. We also construct a thin monolayer of Au NPs on the HOPG substrate by employing same procedure as mention above.

M. Set up parameters for STM imaging and STS

We perform STM imaging and STS in a custom-made low-temperature STM equipped with a UNISOKU Pt-Ir tip (apex radius 10 nm) in a ^{3}He cryostat at 4 K.[13, 14] The STM controller is R9, by RHK Technology[15] with special low-noise current amplifiers (IVP-100 and IVP-300). We execute a slow x-direction scanning to achieve low-noise topography images with (512x512) data points. The topography images are recorded in a constant current mode with the STM feedback loop set to a tunnelling current of 50 pA at 1 V bias voltage for the Au (111) substrate and of 155 pA and 55 mV for HOPG substrate, respectively. Differential conductance (d*I*/d*V*) curves in the tunnelling regime are recorded by placing the STM tip above an individual Au NP and by a current-to-voltage converter with 1 V /nA gain. One d*I*/d*V* spectrum is acquired within 30s. Set-up current and voltage have been set at 2.0 nA and 2.0-2.5 V, respectively, for Au(111) substrate to achieve good stability of the tip during data acquisition. During spectroscopy, the feedback loop is initially adjusted to a higher time constant and a lower gain parameter for the tip stability. Later, throughout the data acquisition, the feedback loop is turned off. In addition, the bias voltage is modulated with the ac voltage, with root-mean-square amplitude of 40 mV and a frequency of 733 Hz for d*I*/d*V* spectra via the lock-in technique. We observe clear SET behaviour, since the total tunnelling resistance (R_{T}) in our experiment is considerably greater (335 MΩ - 1.25 GΩ) than the quantum resistance h/e^2 = 25.8 kΩ (with h Planck's constant

and e the elementary charge). The thermal energy spread ($k_B T$) at 4 K amounts to 0.34 meV and is much lower than the charging energy of a typical Au NP (around 0.4 eV, depending on the size of the NPs). The charging energy equals to e^2/C_{T} where C_{T} is the total capacitance of the junctions of the DBTJ system.

N. Set up for ultrafast spectroscopy

The pump-probe set-up for broadband femtosecond (fs) time-resolved optical spectroscopy is built around a 250 kHz Ti:sapphire amplifier (Coherent REGA 9050) producing 50 fs near-infrared pulses at 800 nm (1.55 eV) central wavelength. Part of the beam is frequency doubled in the BBO crystal, providing 70 fs pump pulses at 400 nm (3.1 eV). White light continuum (WLC) probe pulses, spreading the photon energies between 1.4 and 2.8 eV, are generated by tightly focusing the near-infrared beam onto a 2mm thick, c-axis oriented [001] sapphire.[16] The generated WLC is collected and collimated by a 90 degree off-axis parabolic aluminium mirror. A thin dielectric mirror, highly reflective for 800nm, is placed in the white light beam path, to selectively filter out a large portion of the 800 nm fundamental. A Michelson interferometer type configuration is used to split the WLC beam into two beams, which are both spatially and temporally separated, to serve as a probe and a reference beam, respectively. Another off-axis parabolic mirror focuses the slightly spatially separated WLC beams at near normal incidence onto the sample, with a spot diameter ≤ 90 μm. After passing through the sample, the beams are dispersed by a SF10 prism onto two parallel 32-element photodiode arrays (Hamamatsu S4111-Q). The detection unit is home-built and has a modular circuit board design. The 32-elements of each of the arrays are read-out in parallel and amplified on the first board. The signal voltage output of one array (reference) is inverted. The 64 channels are directed to 32 operational amplifiers on the second board, yielding the voltage difference (signal). The voltage difference is amplified again and lead to the third circuit board connected to a fast 32-channel A/D measurement board (Dewetron ORION 3216) installed in a PC. Wavelength calibration is accomplished by using various band-pass filters placed in the WLC beam. Time-resolved changes in transmission are recorded by varying the time-delay between the pump and WLC probe pulses using a fast-scan delay stage (APE GmbH).

References

1. S. Link and M. A. El-Sayed, *J. Phys. Chem. B* 1999, **103**, 4212-4217.
2. T. Klar, M. Perner, S. Grosse, G. von Plessen, W. Spirkl and J. Feldmann, *Phys. Rev. Lett.*, 1998, **80**, 4249-4252.
3. W. Haiss, N. T. Thanh, J. Aveyard and D. G. Fernig, *Anal. Chem.*, 2007, **79**, 4215-4221.
4. S. Peng, J. M. McMahon, G. C. Schatz, S. K. Graya and Y. Suna, *Proc. Natl. Acad. Sci.,* 2010, **107**, 14530-14534.
5. A. L. Martinez-Hernandez, C. Velasco-Santos and V. M. Castano, *Curr. Nanosci.*, 2010, **6**, 12-39.
6. D. Sarid, *Exploring Scanning Probe Microscopy with MATHEMATICA*, Wiley-VCH Verlag GmbH & Co. KGaA, Germany, 2nd edn., 2007.
7. D. C. Ralph, C. T. Black and M. Tinkham, *Phys. Rev. Lett.*, 1995, **74**, 3241-3244.
8. N. W. Ashcroft, N. D. Mermin, *Solid State Physics,* Cengage Learning US, 1st Ed., 1976.
9. J. G. A. Dubois, E. N. G. Verheijen, J. W. Gerritsen and H. Vankempen, *Phys. Rev. B*, 1993, **48**, 11260-11264.
10. A. E. Hanna and M. Tinkham, *Phys. Rev. B*, 1991, **44**, 5919-5922.
11. M. N. Martin, J. I. Basham, P. Chando and S. K. Eah, *Langmuir*, 2010, **26**, 7410-7417.
12. M. N. Martin, D. W. Li, A. Dass and S. K. Eah, *Nanoscale*, 2012, **4**, 4091-4094.

13. C. Debuschewitz, F. Münstermann, V. Kunej and E. Scheer, *J. Low. Temp. Phys.*, 2007, **147**, 525-535.

14. M. Wolz, C. Debuschewitz, W. Belzig and E. Scheer, *Phys. Rev. B*, 2011, **84**, 104516.

15. http://www.rhk-tech.com/r9plus/.

16. R. R. Alfano, *The Supercontinuum Laser Source: Fundamentals with Updated References*, Springer, U.S.A, 2nd edn., 2006.